Journal of Inclusion Phenomena and Macrocyclic Chemistry **37:** 407–421, 2000.

Switching Ca^{2+}/Ba^{2+} to Ba^{2+}/Ca^{2+} Potentiometric Selectivities of Podands with Phosphoryl-containing Terminal Groups: A Molecular Modelling Study

A. VARNEK[a], T. VOLKOVA[a], O. M. PETRUKHIN[b] and G. WIPFF[a⋆]
[a]*Laboratoire MSM, UMR 7551 CNRS, Université Louis Pasteur, 4, rue B. Pascal, Strasbourg, 67000, France;*
[b]*Russian Mendeleyev University of Chemical Technology, Miusskaya Sq., 9, Moscow, Russia*

(Received: 7 May 1999; in final form: 18 June 1999)

Abstract. It has been shown experimentally that the Ca^{2+}/Ba^{2+} potentiometric selectivity of phosphoryl-containing podand R—O—(CH_2—CH_2—O)$_n$—R, R = —C_6H_4—P(O)Ph_2, n = 3 (**I**), switches to Ba^{2+}/Ca^{2+} when the ligand contains the longer polyether chain, n = 5 (**II**). Here, we report molecular dynamics and free energy perturbation simulations performed using the AMBER 4.1 program on the complexes **L**·M^{2+} (M^{2+} = Ca^{2+}, Sr^{2+} and Ba^{2+}, **L** = **I** and **II**) in the gas phase in order to gain a microscopic insight into structural and energy binding properties of podands as a function of n. Mixed QM/MM (PM3/AMBER) calculations were performed to analyse the role of polarisation effects on the complexation selectivity of podands. It is shown that an increase of n does not affect the interactions of M^{2+} with phosphine oxide groups, but leads to less efficient interactions of small cations with the polyether chain. Calculated potentiometric selectivities of **I** ($Ca^{2+} > Ba^{2+}$) and **II** ($Ba^{2+} > Ca^{2+}$) are in agreement with the experimental data.

Key words: ion-selective electrodes, podands, metal cations, molecular dynamics, QM/MM calculations, binding selectivity, molecular recognition, polarization effects.

1. Introduction

Podands [1, 2] R—O—(CH_2—CH_2—O)$_n$—R with two phosphoryl-containing terminal fragments (R) linked by a polyether chain (**L**, Chart I) represent a promising class of complexing agents. They can be easily modified by varying the substituents at phosphorus and the length of their polyether chain. More than 50 phosphoryl-containing podands with different terminal groups (n = 1–7; R = —CH_2—CH_2—P(O)X_2, —o-C_6H_4—P(O)X_2, —o-C_6H_4—CH_2—P(O)X_2, —CH_2—P(O)X_2 with X = Ph, Alk and O-Alk) have been synthesized and studied as complexing agents in THF : $CHCl_3$ and in acetonitrile solutions (see [3–6] and

⋆ Author for correspondence: Phone 333 884 16071; Fax: 333 884 16104; E-mail: wipff@chimie.u-strasbg.fr

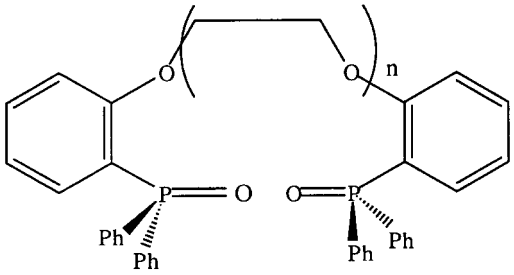

n=3 (**I**); 5 (**II**)

Chart 1. Phosphoryl-containing podands studied by molecular dynamics simulations.

references therein). Extraction by podands of alkali and alkaline earth cations [7–9], lanthanides [10, 11] and actinides [10–12] and a number of transition metals [13–16] has been investigated.

Recently Petrukhin *et al*. examined phosphoryl-containing podands as carriers of alkali [17] and alkaline earth [18] cations in ion selective electrodes (ISE). An interesting result was found for the transport of alkaline earth cations by podands R—O—(CH_2—CH_2—O)$_n$—R, R = —*o*-C_6H_4—P(O)Ph_2 from water to the membrane containing dibutylphthalate as solvent. Podands with a relatively short polyether chain ($n \leq 3$) selectively transport Ca^{2+}, whereas those with longer chains ($n \geq 4$) are selective for Ba^{2+} [18]. From the results obtained in [18] it is not clear whether this switching of selectivity is related to stereochemical effects (formation of optimal coordination polyhedrons or suitable pseudo cavities for metals), to electronic effects (polarization, charge transfer) or to solvation effects. As no structural information on the complexes of these phosphoryl-containing podands with alkaline earth cations is available, the coordination patterns of M^{2+} are not known. This led us to undertake molecular modelling studies in order to analyse the structure–binding affinity relationships on the basis of intra- and intermolecular interactions. Computer experiments can indeed provide microscopic descriptions of molecular systems (structure, energy and dynamics) and macroscopic parameters (thermodynamics of complexation, extraction and transfer). Earlier, molecular mechanics and molecular dynamics studies have been performed on some mono- and tripodands in the gas phase, in solution and at the water/chloroform interface in relation to their complexation [6, 19, 20], extraction [9, 21] and catalytic [22] properties.

Here we report molecular dynamics (MD) and quantum mechanics/molecular mechanics (QM/MM) studies of the complexes of podands **I** (n = 3) and **II** (n = 5) with alkaline earth cations M^{2+} (M^{2+} = Ca^{2+}, Sr^{2+} and Ba^{2+}) aiming to gain microscopic insights into their structure and binding selectivities as a function of n. This is, to our knowledge, the first attempt to estimate potentiometric selectivity coefficients of ISE based on molecular simulations.

The potentiometric selectivity coefficient $K_{\text{pot}}(M_i^{n+}/M_j^{n+})$, measured experimentally by ISE, can be related to the difference between the free energies of transfer ($\Delta\Delta G_{\text{tr}}$)) of cations M_i^{n+} and M_j^{n+} from water into the membrane where they form complexes with **L** [23]

$$-RT \cdot \log K_{\text{pot}}(M_i^{n+}/M_j^{n+}) = \Delta\Delta G_{\text{tr}} = \Delta G_{\text{tr},j} - \Delta G_{\text{tr},i} \tag{1}$$

To estimate the relative free energies $\Delta\Delta G_{\text{tr}}$ we used a method [24, 25] based on the free-energy perturbation technique [26].

Recently [9], we have performed MD simulations on the **II** · M^{2+} and **II** · $M^{2+}(Pic^-)_2$ complexes in the gas phase and in chloroform. It has been shown that this weakly polar solvent does not significantly modify the structure of the complexes compared to the gas phase. Therefore, in this study we assume that structures simulated in the gas phase are similar to those in the dibutylphthalate solvent, used in ISE [18]. No counterion, nor additional components of the membrane (sodium tetraphenylborate [18]) were taken into account in our calculations. This is partially justified by the fact that in ISE the complex is dissociated from the counterion [18]. Despite these simplifications, we have obtained reasonable results concerning the structure of the complexes and the calculated potentiometric selectivities.

2. Method

2.1. FORCE FIELD CALCULATIONS

The AMBER 4.1 software [27] was used for molecular mechanics and molecular dynamics simulations, with the following representation of the potential energy:

$$\begin{aligned} E_{\text{total}} = {} & \Sigma_{\text{bonds}} K_i (r - r_{\text{eq}})^2 + \Sigma_{\text{angles}} K_\theta (\theta - \theta_{\text{eq}})^2 + \\ & + \Sigma_{\text{dihedrals}} V_n (1 + \cos n\phi) \\ & + \Sigma_{i<j} (q_i q_j / R_{ij} - 2\epsilon_{ij} (R^*_{ij}/R_{ij})^6 + \epsilon_{ij} (R^*_{ij}/R_{ij})^{12}). \end{aligned}$$

Here the bonds and bond angles are treated as harmonic springs, and a torsional term is associated with the dihedral angles. The interactions between atoms separated by at least three bonds are described within a pairwise additive 1–6–12 potential. Parameters were taken from the AMBER force field [28]. The electrostatic atomic charges (ESP) [29] of **I** and **II** were calculated using the MNDO method with the MOPAC-5 program [30]. These charges were multiplied by 1.42 to scale them to the *ab initio* 6-31G* values [31].

No scaling of 1–4 nonbonded interactions was used. The cation parameters (ϵ, R^*) were fitted by Åqvist to reproduce relative and absolute free energies of hydration [32]. After 1000 steps of conjugate gradient energy minimization, the MD simulations were run for 200 ps at 300 K using the Verlet algorithm [33], starting with random velocities. The time step was 1 fs, without using SHAKE. A

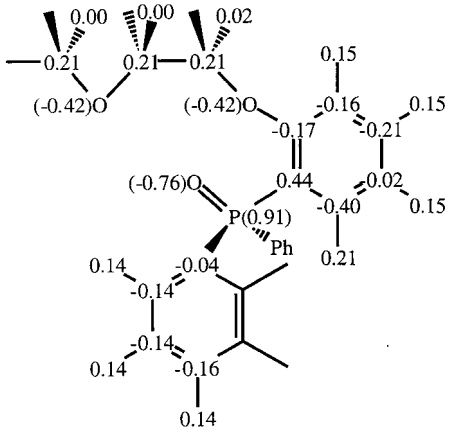

Chart 2. Charge distribution on the podands **I** and **II**.

residue based cutoff of 10 Å was used for nonbonded interactions. The temperature was controlled by velocity scaling in the gas phase.

The 'FEP' (free energy perturbation) calculations were performed with the windowing technique, changing the ϵ, R^* parameters of M^{2+} linearly with λ, as suggested in reference [34]:

$$\epsilon_\lambda = \lambda \cdot \epsilon_{M1} + (1-\lambda) \cdot \epsilon_{M2}; \quad R^*_\lambda = \lambda \cdot R^*_{M1} + (1-\lambda) \cdot R^*_{M2}.$$

We successively mutated $Ca^{2+} \rightarrow Sr^{2+} \rightarrow Ba^{2+}$. The mutation of a given cation M_1^{2+} (free or complexed) to the next one M_2^{2+} was achieved in 11 windows. At each window, 1 ps of equilibration was followed by 4 ps of data collection, and the change of free energy ΔG was averaged from the forward and backward cumulated values.

2.2. ANALYSIS OF THE MD TRAJECTORIES

The cation-ligand interaction energies ($E_{rmM...L}$) and intrinsic energies of the ligand (E_L) have been recalculated from the MD trajectories using the MD_DRAW program [35]. The energy fluctuations are typically 3–5 kcal/mol. To analyse the energy contributions of different molecular fragments in the binding of M^{2+} in the complexes, the podands (**L**) were 'dissected' into a 'chain' fragment —O—(CH_2—CH_2—O)$_n$— and two terminal groups (R = —*o*-C_6H_4—P(O)Ph_2). The coordination number of M^{2+} was obtained by integration of the radial distribution functions (*rdf*) of the oxygen atoms of **L**, around M^{2+}. The effective size of the **L** · M^{2+} complexes was calculated by the radius of gyration defined as: $R^2_{gyr} = (\Sigma R_i^2)/N$, where r_i is the distance between the atom i and the center of mass of the complex, and the summation includes all atoms of **L** · M^{2+}.

2.3. QM/MM CALCULATIONS

Energy minimization of the complexes **I** and **II** with Ca^{2+} and Ba^{2+} were performed using the hybrid quantum mechanics/molecular mechanics (QM/MM) method [36] implemented in the ROAR program [37]. In these calculations, the cation is represented by classical MM method as described above, while for the ligands we used the PM3 semi-empirical method [38], taking account of the electric field of the cation. The van der Waals cation–ligand interactions were treated classically using the AMBER4 force field with the same parameters as in the MD simulations [27, 32]. In this way, a polarization of the ligand in the field of the cation was taken into account. Before QM/MM calculations, all structures were preliminary minimized using the AMBER4 force field.

The ROAR program [37] has been modified to print out the Mulliken charges on the atoms of the ligand.

3. Results

3.1. MOLECULAR DYNAMICS SIMULATIONS IN THE GAS PHASE

In the $\mathbf{I} \cdot M^{2+}$ complexes, the coordination polyhedron of the cation represents a distorted octahedron in which two phosphoryl O_{ph} oxygens occupy axial positions, whereas four O_{eth} atoms lie approximately in the same 'equatorial' plane (Figure 1). The average $M^{2+} \cdots O_{ph}$ distances (2.15, 2.35 and 2.55 Å for the complexes of Ca^{2+},Sr^{2+} and Ba^{2+}, respectively) are shorter by 0.2 Å than the $M^{2+} \cdots O_{eth}$ ones (2.35, 2.55 and 2.77 Å, respectively).

The three $\mathbf{II} \cdot M^{2+}$ complexes have a helix-like shape (Figure 1) where the cation is situated inside the pseudocavity formed by the donor atoms of the ligand. The $M^{2+} \cdots O_{ph}$ distances are practically the same as in the corresponding $\mathbf{I} \cdot M^{2+}$ complexes, whereas interactions between the cation and ether oxygens are less efficient (Table I). In the $\mathbf{II} \cdot Ca^{2+}$ and $\mathbf{II} \cdot Sr^{2+}$ complexes, the cation firmly coordinates to five ether oxygens (2.46 and 2.63 Å, respectively); the sixth one is situated by 0.15–0.20 Å further. In the Ba^{2+} complex, all six distances $Ba^{2+} \cdots O_{eth}$ are similar (2.80 Å).

The radial distribution functions (*rdfs*) of oxygen atoms around the cation characterize the difference between coordination patterns in the $\mathbf{I} \cdot M^{2+}$ and $\mathbf{II} \cdot M^{2+}$ complexes. They display two peaks corresponding to the coordination of M^{2+} to the O_{ph} and to O_{eth} atoms, respectively (Figure 2). For a given cation, the first peaks corresponding to phosphoryl oxygens in **I** and **II** are similarly located, whereas the second peak for the $\mathbf{II} \cdot M^{2+}$ complexes is shifted to larger distances, compared to those for the $\mathbf{I} \cdot M^{2+}$ complexes. The second peaks are generally more diffused than the first ones reflecting the mobility of the $M^{2+} \cdots O_{eth}$ coordination bonds.

Both ligands are flexible enough to adjust themselves to the cation. As a result, the effective radius R_{gyr} of the $\mathbf{L} \cdot M^{2+}$ complex gradually increases with the size of the cation (Table I). Interestingly, the bigger ionophore **II** wraps around M^{2+} in

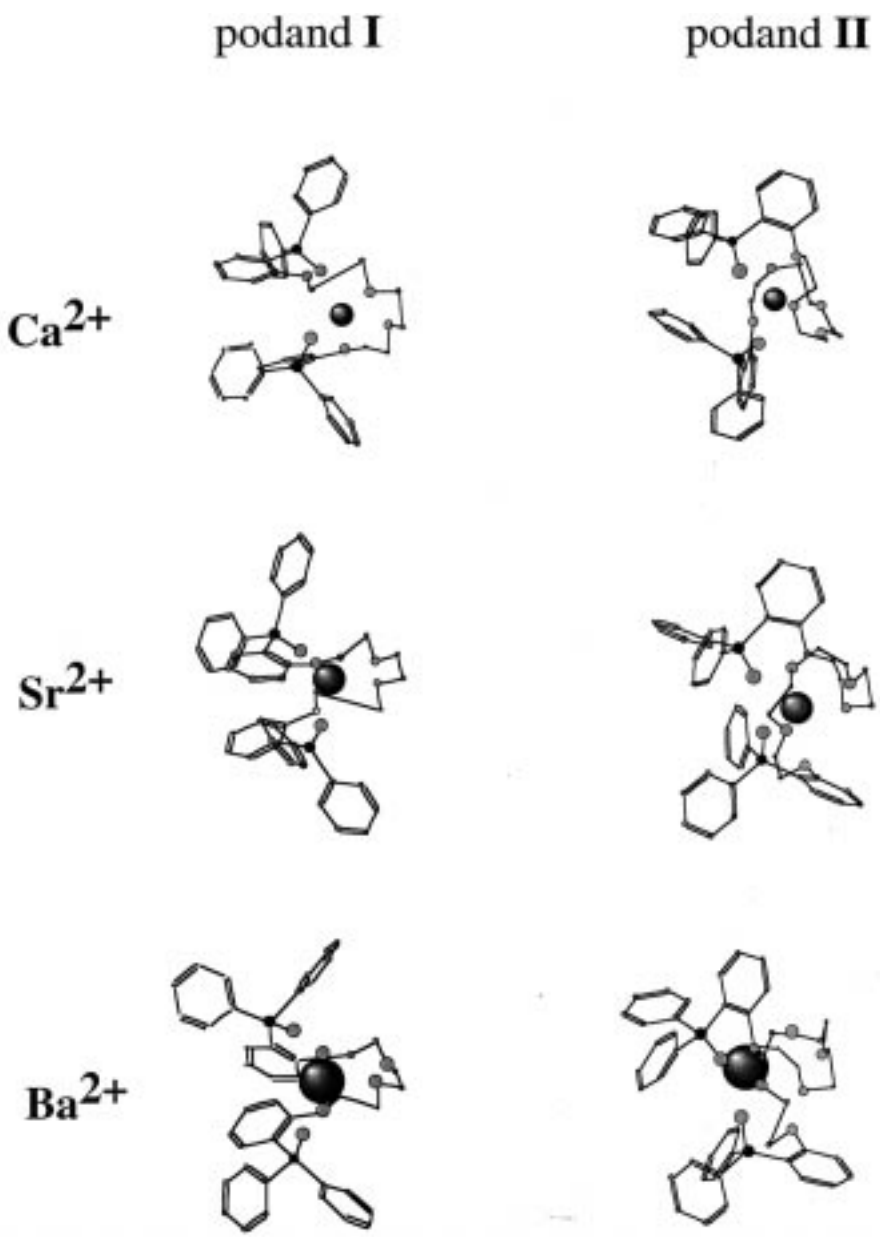

Figure 1. **I** · M^{2+} and **II** · M^{2+} complexes simulated in the gas phase (M^{2+} = Ca^{2+}, Sr^{2+} and Ba^{2+}). Snapshots after 200 ps of MD.

Table I. Geometry[a] and energy[b] characteristics of $\mathbf{I} \cdot M^{2+}$ and $\mathbf{II} \cdot M^{2+}$ complexes ($M^{2+} = Ca^{2+}$, Sr^{2+} and Ba^{2+}) simulated in the gas phase (classical MD). Average after 200 ps

	Podand **I**			Podand **II**		
	Ca^{2+}	Sr^{2+}	Ba^{2+}	Ca^{2+}	Sr^{2+}	Ba^{2+}
R_{gyr}[c]	5.14	5.24	5.51	5.05	5.14	5.25
$M^{2+} \cdots O_{ph}$	2.15	2.35	2.55	2.17	2.35	2.56
$M^{2+} \cdots O_{eth}$	2.35	2.55	2.77	2.46; 2.70[d]	2.63; 2.75[d]	2.80
$E_{M \cdots O_{eth}}$	−199	−169	−149	−240	−215	−189
$E_{M \cdots O_{ph}}$	−117	−94	−78	−121	−95	−80
$E_{M \cdots \mathbf{L}}$	−316	−263	−227	−361	−310	−269
$E_{\mathbf{L}}$	476	467	461	549	535	526
$E_{[M\mathbf{L}]}$	160	204	234	188	225	257

[a] Distances (Å) between M^{2+} and oxygens of the phosphoryl groups ($M^{2+} \cdots O_{ph}$) and of the polyether chain ($M^{2+} \cdots O_{eth}$). Statistical fluctuations are 0.05–0.10 Å.

[b] Interaction energies (kcal/mol) for cation-terminal groups ($E_{M \cdots O_{ph}}$), cation–'chain' fragment ($E_{M \cdots O_{eth}}$), cation–ligand ($E_{M \cdots \mathbf{L}}$). Intrinsic energies of the ligand ($E_{\mathbf{L}}$), total energy of the complex ($E_{[M\mathbf{L}]} = E_{M \cdots \mathbf{L}} + E_{\mathbf{L}}$). Statistical fluctuations are 3–7 kcal/mol.

[c] Radius of gyration (R_{gyr}) in Å.

[d] The first number corresponds to the five firmly bound ether oxygens, the second number corresponds to the weakly bound O_{eth}) atom.

a more compact way than **I** does: for a given cation, R_{gyr} of the $\mathbf{I} \cdot M^{2+}$ complexes is larger than that of the $\mathbf{II} \cdot M^{2+}$ complexes.

The energy component analysis shows that in the $\mathbf{I} \cdot M^{2+}$ and $\mathbf{II} \cdot M^{2+}$ complexes, the interaction energies of a given M^{2+} with the —C_6H_4—$P(O)Ph_2$ terminal groups ($E_{M \cdots O_{ph}}$) are similar (Table I). This is consistent with the similarity of the corresponding $M^{2+} \cdots O_{ph}$ distances. Although the total cation–polyether chain interaction energies ($E_{M \cdots O_{eth}}$) are larger for the $\mathbf{II} \cdot M^{2+}$ complexes than for the $\mathbf{I} \cdot M^{2+}$ complexes, we notice that the average interactions per O_{eth} atom ($E_{M \cdots O_{eth}}/N$, where N is the number of O_{eth} atoms), are more effective for the smaller podand (Figure 3). It also corresponds to smaller $M^{2+} \cdots O_{eth}$ distances in the $\mathbf{I} \cdot M^{2+}$ complexes compared to the $\mathbf{II} \cdot M^{2+}$ complexes (Table I and Figure 2).

Energy parameters given in Table I show that the relative contribution of the terminal groups to the total cation–ligand interactions ($E_{M \cdots O_{ph}}/E_{M \cdots L}$) decreases with the size of the cation. Indeed, this ratio is 0.37, 0.36 and 0.34 (**I**) and 0.34, 0.31 and 0.30 (**II**) for the complexes of Ca^{2+}, Sr^{2+} and Ba^{2+}, respectively.

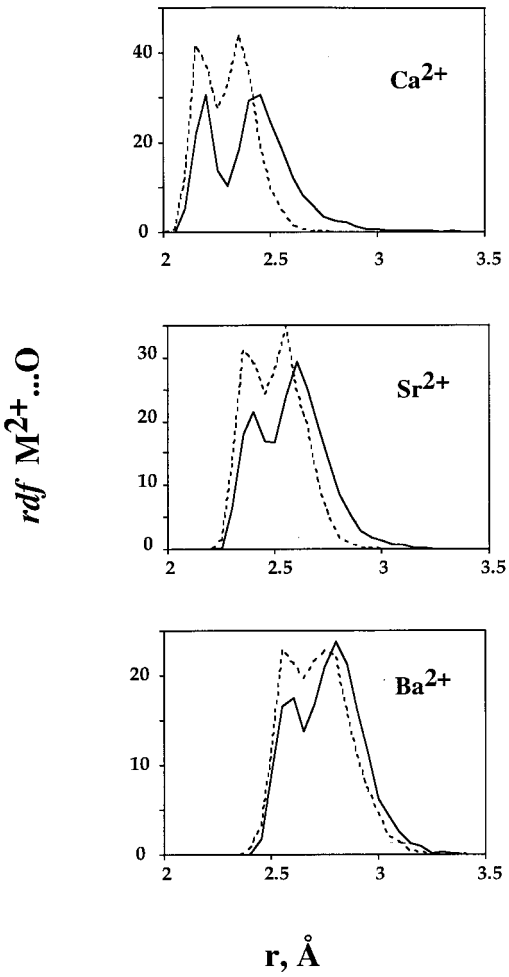

Figure 2. Radial distribution functions $M^{2+}\cdots O$ for the $\mathbf{I}\cdot M^{2+}$ (dashed line) and $\mathbf{II}\cdot M^{2+}$ (solid line) complexes simulated in the gas phase (M^{2+} = Ca^{2+}, Sr^2, and Ba^{2+}).

4. Potentiometric Selectivity of Podands from Free Energy Perturbation Simulations

To estimate the potentiometric selectivity coefficients according to (1), we calculated relative free energies $\Delta\Delta G_{\text{tr}}$ of transfer of M^{2+} ions from an aqueous to an organic solution, using the thermodynamic cycle presented in Scheme 1 [24, 25].

$$\begin{array}{ccc} \mathbf{L}_{\text{org}} + \mathrm{M}^{2+}_{1,\text{wat}} & \xrightarrow{\Delta G_{\text{tr},1}} & [\mathbf{L}\mathrm{M}^{2+}_{1}]_{\text{org}} \\ \downarrow \Delta G_{3,\text{wat}} & & \downarrow \Delta G_{4,\text{org}} \\ \mathbf{L}_{\text{org}} + \mathrm{M}^{2+}_{2,\text{wat}} & \xrightarrow[\Delta G_{\text{tr},2}]{} & [\mathbf{L}\mathrm{M}^{2+}_{2}]_{\text{org}} \end{array}$$

Scheme 1

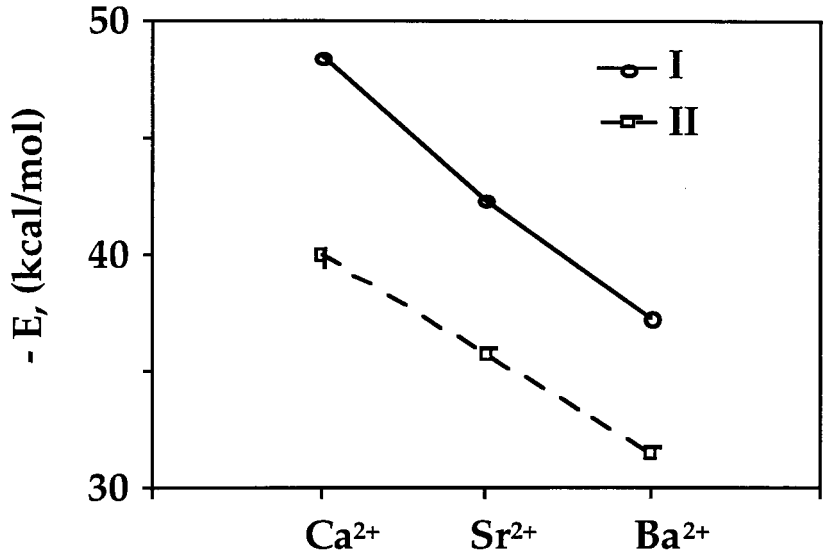

Figure 3. Average energies (kcal/mol) of interaction between M^{2+} (M^{2+} = Ca^{2+}, Sr^2, and Ba^{2+}) and the polyether chain in the **I** · M^{2+} and **II** · M^{2+} complexes *per ether oxygen.*

This model assumes that (i) the free ions are present in water only, (ii) the charged **L** · M^{2+} complexes are entirely in the organic phase. The selectivity of extraction is given by

$$\Delta\Delta G_{\text{tr}} = \Delta G_{\text{tr},1} - \Delta G_{\text{tr},2} = \Delta G_{3,\text{wat}} - \Delta G_{4,\text{org}}. \tag{2}$$

Calculations [9] performed on the **II** · M^{2+} complexes showed that their geometry in the gas phase and in chloroform are similar, and that they are similarly solvated. Therefore, for the weakly polar dibutylphthalate solvent, one may approximate $\Delta G_{4,\text{org}}$ by $\Delta G_{4,gas}$.

The relative free energies calculated according to Scheme 1 and Equation (2) are given in Table II. One can see that intrinsically ($\Delta G_{4,\text{gas}}$) both podands interact best with the smallest Ca^{2+} cation in the order $Ca^{2+} > Sr^{2+} > Ba^{2+}$. The selectivity order $Ca^{2+} > Ba^{2+}$ (for **I**) and $Ba^{2+} > Ca^{2+}$ (for **II**) in the biphasic system is reproduced computationally only if the dehydration energy of cations ($\Delta G_{3,\text{wat}}$) is taken into account. Thus, the potentiometric selectivity results from an interplay between the binding affinity of the ionophore in the organic phase and the dehydration energy of the cations.

Experimental and calculated potentiometric coefficients $\log K_{\text{pot}}(Ba^{2+}/Ca^{2+})$ for **I** and **II** are presented in Figure 4. Although, the experimental values were not reproduced quantitatively, the calculations give the correct trend of the potentiometric selectivities of podands as a function of the length of polyether chain n: **I** is selective for Ca^{2+}, whereas **II** is selective for Ba^{2+}.

Table II. Relative free energies of mutation (kcal/mol) of Ca^{2+}, Sr^{2+}, Ba^{2+}, uncomplexed and complexed by podands **I** and **II**[a]

	Podand **I**			Podand **II**		
	$Ca^{2+} \rightarrow Sr^{2+}$	$Sr^{2+} \rightarrow Ba^{2+}$	$Ca^{2+} \rightarrow Ba^{2+}$	$Ca^{2+} \rightarrow Sr^{2+}$	$Sr^{2+} \rightarrow Ba^{2+}$	$Ca^{2+} \rightarrow Ba^{2+}$
ΔG_4 (complexed M^{2+})[a]	37.5/37.7	29.9/29.7	67.4	34.7/34.6	30.8/31.1	65.5
ΔG_3 (free M^{2+}) in water[b]	34.9	30.8	65.7	34.9	30.8	65.7
$\Delta\Delta G_{tr}$, calcul	−2.7	1.0	−1.7	0.3	−0.1	0.2
$\Delta\Delta G_{tr}$, experimental[c]			−1.0			0.5

[a] Calculations in the gas phase. The two numbers correspond to 'forward' and 'backward' mutations.
[b] Experimental values from reference [39].
[c] Experimental free energies derived from the potentiometric selectivity coefficients from reference [18].

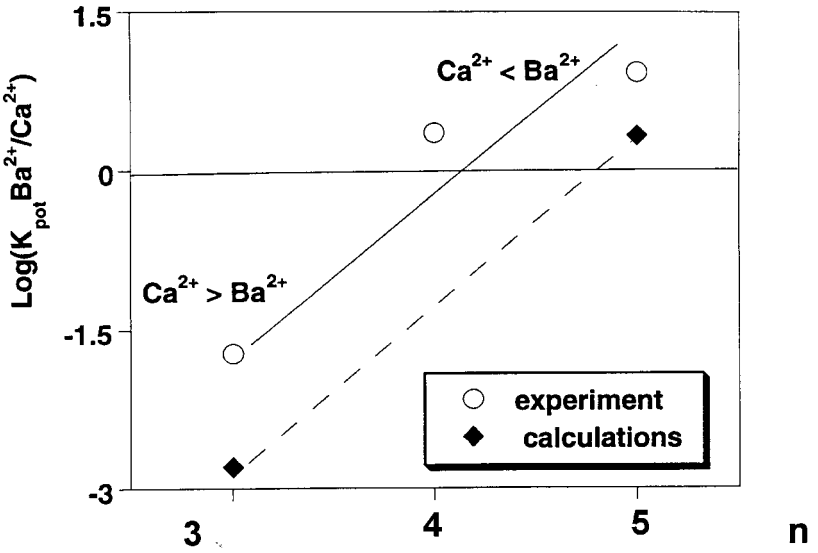

Figure 4. Experimental and calculated potentiometric Ba^{2+}/Ca^{2+} selectivities of podands **I** and **II** R—O—$(CH_2—CH_2—O)_n$—R, R = —*o*-C_6H_4—$P(O)Ph_2$, n = 3–5.

5. Discussion

5.1. RELATIONSHIPS BETWEEN STRUCTURE AND BINDING SELECTIVITY OF PODANDS

It follows from Table II that switching of Ca^{2+}/Ba^{2+} to Ba^{2+}/Ca^{2+} selectivities is related to the reduction from 67.4 kcal/mol (podand **I**) to 65.5 kcal/mol (podand **II**) of the *relative* binding affinity ($\Delta G_4(Ca^{2+}/Ba^{2+})$) of the ligand with n. Here we rationalize this effect in terms of geometry and energy parameters given in Table I. It can be seen (Table I) that the interaction energies between the cation and the terminal groups, $E_{M\cdots O_{ph}}$, are practically the same for the $\mathbf{I} \cdot M^{2+}$ and $\mathbf{II} \cdot M^{2+}$ complexes, i.e., the 'switching' effect is mostly related to the interactions of M^{2+} with the polyether chain. In the $\mathbf{L} \cdot M^{2+}$ complexes, the smaller ligand **I** forms shorter $M^{2+}\cdots O_{eth}$ coordination bonds than ligand **II**. The difference between $M^{2+}\cdots O_{eth}$ distances in $\mathbf{L} \cdot M^{2+}$ varies as a function of cation size: it ranges from 0.15 Å for Ca^{2+} to 0.03 Å for Ba^{2+}. Two important features follow from these observations: (i) each O_{eth} atom in $\mathbf{II} \cdot M^{2+}$ interacts with the cation less efficiently than in $\mathbf{I} \cdot M^{2+}$, and (ii) this phenomenon is more important for the complexes of Ca^{2+} than of Ba^{2+}. In addition, Figure 3 shows that the cation–'chain' interaction energy per O_{eth} atom is larger for $\mathbf{I} \cdot M^{2+}$ than for $\mathbf{II} \cdot M^{2+}$.

Thus, an increase of the length of the polyether chain n does not modify cation-terminal group interactions, but modulates the cation–chain interactions as a function of the cation's size and, hence, modulates cation binding selectivities of podands.

5.2. QM/MM CALCULATIONS ON **l** · M^{2+} COMPLEXES. POLARIZATION EFFECTS ON COMPLEXATION SELECTIVITY OF PODANDS

Electronic polarization effects were not included in our MD and FEP simulations, although they can play an important role in the metal binding selectivity of podands bearing readily polarizable phosphoryl and aromatic fragments. Quantitatively, it is not clear whether taking polarization into account increases the gap between relative free energies $\Delta G_4(Ca^{2+}/Ba^{2+})$ for **I** and **II**, thus favouring the switching of Ca^{2+}/Ba^{2+} to Ba^{2+}/Ca^{2+} complexation selectivity of podands with n. In order to rationalise these effects, we performed calculations on the uncomplexed ligands **I** and **II** and their complexes with $M^{2+} = Ca^{2+}$ and Ba^{2+} using the mixed QM/MM (PM3/AMBER) method. Although, the current version [37] of the QM/MM program ROAR is not able to perform free energy calculations, some conclusions about polarization effects on binding selectivity of podands could be drawn using the minimized energies of the complexes.

Data given in Table III show that QM/MM calculations lead to $M^{2+} \cdots O_{ph}$ and $M^{2+} \cdots O_{eth}$ distances some of which are practically the same, while others are smaller by 0.02–0.03 Å than those obtained in force field calculations.

Interactions with M^{2+} in the complexes lead to the shift of the electron density of a ligand **L** toward its donor atoms; this effect is stronger for the smaller cation. Thus, the Mulliken charges on the O_{ph} atoms increase from -0.85 for the uncomplexed podands to -1.23 (**L** · Ca^{2+}) and to -1.16 (**L** · Ba^{2+}). A similar trend is observed for the O_{eth} atoms: their charges varies, on average, from -0.25 (**L**), to -0.45 (**L** · Ca^{2+}) and to -0.40 (**L** · Ba^{2+}). Ab initio QM calculations also demonstrate such polarization of the coordinated ligand [40].

The relative energies of the complexes $E_{rel}(Ca^{2+}/Ba^{2+}) = E_{[Ca\cdot\mathbf{L}]} - E_{[Ba\cdot\mathbf{L}]}$ calculated by the QM/MM method (-89.8 and -82.7 kcal/mol for **I** and **II** respectively) are larger than the AMBER values (-74.6 and -71.8 kcal/mol, Table III). The gap between these values is larger with QM/MM (7.2 kcal/mol) than with AMBER (2.8 kcal/mol), showing that polarization of the ligand favours the switching of Ca^{2+}/Ba^{2+} to Ba^{2+}/Ca^{2+} complexation selectivity of podands with n.

6. Conclusions

This work is devoted to theoretical studies of the transfer of alkaline earth cations by podands R—O—$(CH_2$—CH_2—$O)_n$—R with terminal phosphoryl groups from water to a weakly polar solvent.

According to MD simulations, the coordination patterns of **I** · M^{2+} and **II** · M^{2+} ($M^{2+} = Ca^{2+}$, Sr^{2+}, Ba^{2+}) complexes differ. In the former, the cation has an octahedral environment, where axial positions are occupied by the oxygens of phosphoryl groups. In the latter, the complexes have a helix-like shape. An increase of the length (n) of the polyether chain does not affect the energetics of M^{2+}–terminal group interactions. On the other hand, the cation-ether oxygen interaction

Table III. Geometry[a] and energy[b] characteristics of **I** · M^{2+} and **II** · M^{2+} complexes (M^{2+} = Ca^{2+} and Ba^{2+}) in the gas phase obtained after energy minimization using AMBER4 force field (MM) and PM3/AMBER (QM/MM) methods

	Podand **I**				Podand **II**			
	Ca^{2+}		Ba^{2+}		Ca^{2+}		Ba^{2+}	
	MM	QM/MM	MM	QM/MM	MM	QM/MM	MM	QM/MM
$M^{2+}\cdots O_{ph}$	2.14	2.08	2.52	2.45	2.16	2.11	2.53	2.48
$M^{2}\cdots O_{eth}$	2.33	2.33	2.69	2.67	2.41	2.46	2.77	2.80
					2.52[c]	2.75[c]		
$E_{M\cdots O_{eth}}$	−196.6		−151.9		−249.0		−194.5	
$E_{M\cdots O_{ph}}$	−119.7		−76.1		−120.1		−79.6	
$E_{M\cdots \mathbf{L}}$	−316.3	−377.5	−228.0	−271.8	−370	−417.8	−274.1	−306.1
$E_{\mathbf{L}}$	401.1	−4.4	387.4	−20.3	466.3	−61.2	442.4	−90.2
$E_{[M\mathbf{L}]}$	84.9	−381.9	159.4	−292.1	96.4	−479.0	168.2	−396.3
	MM		QM/MM		MM		QM/MM	
$E_{rel}(Ca^{2+}/Ba^{2+})$	−74.6		−89.8		−71.8		−82.7	

[a] Average distances (Å) between M^{2+} and oxygens of the phosphoryl groups ($M^{2+}\cdots O_{ph}$) and of the polyether chain ($M^{2+}\cdots O_{eth}$).

[b] Total ($E_{[M\mathbf{L}]}$) and relative ($E_{rel}(Ca^{2+}/Ba^{2+}) = E_{[Ca\cdot\mathbf{L}]} - E_{[Ba\cdot\mathbf{L}]}$) energies of the complexes, kcal/mol.

[c] The first number corresponds to the five firmly bound ether oxygens, the second number corresponds to the weak bound O_{eth} atom.

energies per O_{eth} atom decrease with n, and change as a function of the cation's size. The variation of n may therefore modulate the binding selectivity of podands.

Molecular dynamics and free energy simulations, and quantum mechanics/molecular mechanics calculations show that both podands intrinsically have a greater affinity for Ca^{2+} than for Ba^{2+}. Experimental binding selectivities are reproduced when dehydration energies of cations are taken into account. The switching of Ba^{2+}/Ca^{2+} (for podand **I**, n = 3) into Ba^{2+}/Ca^{2+} (for podand **II**, n = 5) potentiometric selectivities is explained by the fact that both ligands bind both cations similarly via their phosphoryl oxygens. As a result, the ether chain of **II** is somewhat too long to efficiently wrap around the smallest cation Ca^{2+}. The agreement between the calculated and experimental potentiometric selectivities is encouraging and suggests that such computer simulations should play an increasing role in the prediction of potentiometric selectivities.

Acknowledgements

This work was supported by the INTAS-94-3249 grant. We thank IDRIS and Louis Pasteur University of Strasbourg for allocation of computer time and Etienne Engler for the modifications to the ROAR program.

References

1. F. Vögtle: *Supramolecular Chemistry*. Wiley, Chichester etc. (1991).
2. G. W. Gokel and O. Murillo: In J. L. Atwood, J. E. D. Davis, D. D. MacNicol, and F. Vögtle (eds.), *Comprehensive Supramolecular Chemistry*, Vol. 2, Pergamon (1996), pp. 1–33.
3. V. I. Evreinov, Z. N. Vostroknutova, A. N. Bovin, A. N. Degtyarev, and E. N. Tsvetkov: *Z. Obshch. Khim. (Russ.)* **60**, 1506 (1990) (110: 219964r).
4. A. N. Bovin, V. I. Evreinov, Z. V. Safronova, and E. N. Tsvetko: *Russ. Chem. Bull.* **42**, 912–916 (1993).
5. V. P. Solovev, O. A. Govorkova, O. A. Raevskii, V. E. Baulin, V. K. Syundyukov, and E. N. Tsvetkov: *Bull. Acad. Sci. USSR, div. Chem. Sci.* **40**, 497.
6. V. P. Solov'ev, V. E. Baulin, N. N. Strakhova, V. P. Kazachenko, R. P. Ozerov, V. K. Belsky, A. A. Varnek, T. A. Volkova, and G. Wipff: *J. Chem. Soc., Perkin Trans. 2*, 1249 (1998).
7. A. Y. Tsivadze, S. V. Bondareva, A. V. Levkin, V. E. Baulin, and E. N. Tsvetkov: *Z. Neorg. Khim. (Russ.)* **38**, 1251 (1993) (119: 279984t).
8. A. Y. Tsivadze, A. V. Levkin, S. V. Bondareva, V. E. Baulin, and E. N. Tsvetkov: *Russ. J. Inorg. Chem.* **36**, 1378 (1990).
9. A. Y. Nazarenko, V. E. Baulin, A. Varnek, T. Volkova, G. Wipff, and D. Lamb: *J. Solv. Extr.* **17**, 495 (1999).
10. I. V. Smirnov, T. I. Efremova, A. Y. Shadrin, V. E. Baulin, and E. N. Tsvetkov: *Radiochemistry* **35**, 56 (1993) (119: 104241w).
11. V. A. Karandashev, and V. E. Baulin: *Solvent Extraction and Ion Exchange* **14**, 227 (1996).
12. A. N. Turanov, V. K. Karandashev, V. E. Baulin, and E. N. Tsvetkov: *Radiochemistry (Russ.)* **37**, 128 (1995) (124: 99119j).
13. A. N. Turanov, V. E. Baulin, A. V. Kharitonov, and E. N. Tsvetkov: *Zh. Neorg. Khim. (Russ.)* **39**, 1394 (1994) (121: 239346w).

14. A. N. Turanov, N. K. Evseeva, V. E. Baulin, and E. N. Tsvetkov: *Zh. Neorg. Khim. (Russ.)* **40**, 861 (1995) (123: 153906h).
15. A. N. Turanov, V. E. Baulin, A. F. Solotnov, and E. N. Tsvetkov: *Zh. Neorg. Khim. (Russ.)* **40**, 866 (1995) (123: 153907j).
16. A. N. Turanov, V. E. Baulin, A. V. Kharitonov, and E. N. Tsvetkov: *Zh. Neorg. Khim. (Russ.)* **40**, 866 (1995) (121: 239346w).
17. O. M. Petrukhin, E. V. Shipulo, S. A. Krylova, S. L.. Rogatinskaya, A. F. Zhukov, S. Wilke, H. Muller, E. N. Tsvetkov, V. E. Baulin, V. K. Syundyukova, and N. A. Bondarenko: *J. Anal. Chem. (Engl. Tr.)* **49**, 1175 (1994).
18. O. M. Petrukhin, A. B. Kharitonov, Y. I. Urusov, E. V. Schipulo, N. Y. Kruchinina, and V. E. Baulin: *Anal. Chim. Acta* **353**, 11 (1997).
19. A. A. Varnek, G. Morosi, and A. Gamba: *J. Phys. Org. Chem.* **5**, 109 (1992).
20. A. A. Varnek, J. E. ten Elshof, A. S. Glebov, V. P. Solov'ev, V. E. Baulin, and E. N. Tsvetkov: *J. Mol. Struct.* **271**, 311 (1992).
21. A. Varnek, L. Troxler, and G. Wipff: *Chem. Eur. J.* **3**, 552 (1997).
22. A. A. Varnek, A. Maya, D. Landini, A. Gamba, G. Morosi, and G. Podda: *J. Phys. Org. Chem.* **6**, 113 (1993).
23. W. E. Morf: *The Principles of Ion-Selective Electrodes and of Membrane Transport*, Akademiai Kiado, Budapest (1981).
24. A. Varnek and G. Wipff: *J. Comput. Chem.* **17**, 1520 (1996).
25. G. Wipff and M. Lauterbach: *Supramol. Chem.* **6**, 187 (1995). M. Lauterbach and G. Wipff: in *Physical Supramolecular Chemistry*; L. Echegoyen A. Kaifer (ed.), Kluwer Academic Publishers, Dordrecht, p. 65 (1996).
26. P. Kollman: *Chem. Rev.* **93**, 2395 (1993).
27. D. A. Pearlman, D. A. Case, J. C. Caldwell, W. S. Ross, D. M. Ferguson, G. L. Seibel, U. C. Singh, P. K. Weiner, and P. A. Kollman: AMBER4.1, University of California, CA, San Francisco (1995).
28. W. D. Cornell, P. Cieplak, C. I. Bayly, I. R. Gould, K. M. Merz, D. M. Ferguson, D. C. Spellmeyer, T. Fox, J. W. Caldwell, and P. A. Kollman: *J. Am. Chem. Soc.* **117**, 5179 (1995).
29. F. A. Momany: *J. Phys. Chem.* **82**, 592 (1978).
30. MOPAC-5. QCPE Program No. 589 (1990).
31. B. H. Besler, K. M. J. Merz, and P. A. Kollman: *J. Comput. Chem.* **11**, 431 (1990).
32. J. Åqvist: *J. Phys. Chem.* **94**, 8021 (1990).
33. M. P. Allen and D. J. Tildesley: *Computer Simulation of Liquids*, Clarendon Press, Oxford (1987).
34. U. C. Singh, F. K. Brown, P. A. Bash, and P. A. Kollman: *J. Am. Chem. Soc.* **109**, 1607 (1987).
35. E. Engler and G. Wipff: MD-DRAW. *A Program for the Graphical Representation of Molecular Trajectories*, Université Louis Pasteur: Strasbourg (1992).
36. R. V. Stanton, L. R. Little, and K. M. Merz: *J. Phys. Chem.* **99**, 483 (1995).
37. A. Cheng, R. S. Stanton, J. J. Vincent, K. V. Domodaran, S. L. Dixon, D. S. Hartsough, M. Mori, S. A. Best, and K. M. Merz: ROAR 1.0, Pennsylvania State University (1997).
38. J. J. P. Stewart: *J. Comput. Chem.* **10**, 209 (1989).
39. M. A. Burgess: *Metal Ions in Solution*, Ellis Horwood, Chichester (1978).
40. L. Troxler, A. Dedieu, F. Hutschka, and G. Wipff: *J. Mol. Struct. (THEOCHEM)* **431**, 151 (1998). F. Hutschka, L. Troxler, A. Dedieu, and G. Wipff: *J. Phys. Chem. A* **102**, 3773 (1998). F. Berny, N. Muzet, L. Troxler, A. Dedieu, and G. Wipff: *Inorg. Chem.* **38**, 1244 (1999).